NASA/TM—2019-220216

Optical Array Versus Monolithic Telescope Ground Station Cost Assessment

Robert R. Romanofsky
Glenn Research Center, Cleveland, Ohio

October 2019

NASA STI Program . . . in Profile

Since its founding, NASA has been dedicated to the advancement of aeronautics and space science. The NASA Scientific and Technical Information (STI) Program plays a key part in helping NASA maintain this important role.

The NASA STI Program operates under the auspices of the Agency Chief Information Officer. It collects, organizes, provides for archiving, and disseminates NASA's STI. The NASA STI Program provides access to the NASA Technical Report Server—Registered (NTRS Reg) and NASA Technical Report Server—Public (NTRS) thus providing one of the largest collections of aeronautical and space science STI in the world. Results are published in both non-NASA channels and by NASA in the NASA STI Report Series, which includes the following report types:

- TECHNICAL PUBLICATION. Reports of completed research or a major significant phase of research that present the results of NASA programs and include extensive data or theoretical analysis. Includes compilations of significant scientific and technical data and information deemed to be of continuing reference value. NASA counter-part of peer-reviewed formal professional papers, but has less stringent limitations on manuscript length and extent of graphic presentations.

- TECHNICAL MEMORANDUM. Scientific and technical findings that are preliminary or of specialized interest, e.g., "quick-release" reports, working papers, and bibliographies that contain minimal annotation. Does not contain extensive analysis.

- CONTRACTOR REPORT. Scientific and technical findings by NASA-sponsored contractors and grantees.

- CONFERENCE PUBLICATION. Collected papers from scientific and technical conferences, symposia, seminars, or other meetings sponsored or co-sponsored by NASA.

- SPECIAL PUBLICATION. Scientific, technical, or historical information from NASA programs, projects, and missions, often concerned with subjects having substantial public interest.

- TECHNICAL TRANSLATION. English-language translations of foreign scientific and technical material pertinent to NASA's mission.

For more information about the NASA STI program, see the following:

- Access the NASA STI program home page at http://www.sti.nasa.gov

- E-mail your question to help@sti.nasa.gov

- Fax your question to the NASA STI Information Desk at 757-864-6500

- Telephone the NASA STI Information Desk at 757-864-9658

- Write to:
  NASA STI Program
  Mail Stop 148
  NASA Langley Research Center
  Hampton, VA 23681-2199

NASA/TM—2019-220216

Optical Array Versus Monolithic Telescope Ground Station Cost Assessment

Robert R. Romanofsky
Glenn Research Center, Cleveland, Ohio

Prepared for the
Directed Energy Systems Symposium
sponsored by the Directed Energy Professional Society
Norfolk, Virginia, September 12–16, 2016

National Aeronautics and
Space Administration

Glenn Research Center
Cleveland, Ohio 44135

October 2019

Acknowledgments

This work was supported by the NASA Space Communications and Navigation Office.

Level of Review: This material has been technically reviewed by technical management.

Available from

NASA STI Program
Mail Stop 148
NASA Langley Research Center
Hampton, VA 23681-2199

National Technical Information Service
5285 Port Royal Road
Springfield, VA 22161
703-605-6000

This report is available in electronic form at http://www.sti.nasa.gov/ and http://ntrs.nasa.gov/

Optical Array Versus Monolithic Telescope Ground Station Cost Assessment

Robert R. Romanofsky
National Aeronautics and Space Administration
Glenn Research Center
Cleveland, Ohio 44135

Abstract

The purpose of this study is to outline the design of an optimal array of optical telescopes to emulate performance of a monolithic 12 m telescope in support of deep-space communications. In this case, optimal means minimizing the initial capital investment and operational cost while maintaining performance requirements of the deep-space link. The design is approached from a practical, engineering perspective. Pulse position modulation (PPM) signal formatting and photon counting detectors are assumed at each telescope in the array. That is, the telescopes function as so-called light buckets, so direct detection (as opposed to coherent reception) of the received signals is assumed, and there is no intention to consider active compensation for atmospheric turbulence-induced phase fluctuations. A parametric analysis among aperture size, detector size, and primary mirror surface quality, in the context of field-of-view expansion, is presented to minimize the cost function.

Introduction

The purpose of this study is to outline the design of an optimal array of optical telescopes to emulate performance of a monolithic 12 m telescope in support of deep-space communications. In this case, optimal means minimizing the initial capital investment and operational cost while maintaining performance requirements of the deep-space link. The design is approached from a practical, engineering perspective. Pulse position modulation (PPM) signal formatting and photon counting detectors are assumed at each telescope in the array. That is, the telescopes function as so-called light buckets, so direct detection (as opposed to coherent reception) of the received signals is assumed, and there is no intention to consider active compensation for atmospheric turbulence-induced phase fluctuations. Turbulence can significantly increase the telescope field-of-view over the classic diffraction limit of the primary aperture thereby increasing background photon count without necessarily improving signal power. A parametric analysis among aperture size, detector size, and primary mirror surface quality, in the context of field-of-view expansion, is presented to minimize the cost function. The relationship between PPM slot width and noise is not considered here (i.e., no attempt is made to optimize PPM modulation order in the context of minimizing noise). Besides potentially very substantial cost savings, other advantages of a telescope array include: minimal gravitational effects (i.e., primary mirror/sub-reflector structural sag), reliability through redundancy, and scalability. A possible drawback of a large telescope array is the complexity associated with synchronization of the individual telescope PPM signals.

Part I focusses on estimating the aperture size and number of apertures required to emulate the 12 m aperture and the ensuing cost based on an established cost model derived from empirical data. The analysis does extend that model to include the cryogenic refrigeration initial capital investment and life cycle costs. Part II modifies the analysis by addressing more realistic manufacturing issues, especially mirror surface quality as a cost tradeoff, and uses a previously developed point spread function approach. Specifically, it considers the equivalent telescope aperture, with slight imperfections, that could theoretically perform as well as a diffraction limited (flawless) telescope. Finally, Part III merges both sections and develops a cost minimization strategy.

Part I. Archetype Cost Model

An estimate of the optimal size of optical apertures and the number of such apertures to rival the performance of a single monolithic telescope is provided here. Nonrecurring engineering costs and other sunk costs (e.g., real estate/site development) are excluded for the moment but are regarded as constants that would not alter the shapes or minima of the cost curves to be presented. As a placeholder, it was reported in Reference 15 that an adequate allocation for annual operating costs of an optical observatory facility is about 4 percent of the construction cost.

Cost versus performance models for ground based telescopes have been developed (Refs. 1 and 2). Telescope arraying was not included in the analysis given in Reference 1. Extracted from existing data, the cost was modeled as:

$$C_T = \alpha D^x \tag{1}$$

where C_T is the cost in millions of dollars, D is the telescope diameter in meters, and x is a parameter that varies between 2.4 and 2.8. (Note that in microwave dish models this value is ≈2.8.) This cost includes telescope mount and pointing controls. According to Reference 1, the value of α is a function of "blur circle diameter" which is essentially resolution in arcseconds, designated as "F." From Reference 1, $\alpha = F^{-0.94}/9.15 \approx 1/(10F)$. It is important to understand that α is inextricably linked to the figure and surface quality of the primary mirror. A 10 m telescope with a surface quality corresponding to a 2 μrad field of view might cost about \$80M. Since the telescope functions as a light bucket, a larger diameter telescope with a wider field of view (degraded surface quality) could cost less than a precision smaller telescope. Cost rises sharply as narrower fields of view are required. In Reference 2 it was reported that a 15 m telescope with a 30 μrad field of view (15 times greater surface error) would provide equivalent performance at a cost of about \$20M. One can intuitively interpret α in terms of Strehl loss ≈ exp-$(2\pi\delta/\lambda)^2$, where δ is the rms wave-front error averaged over the aperture and λ is the optical wavelength. For example, if $\delta = 0.01\lambda$, the corresponding Strehl loss is negligible. If $\delta = 0.15\lambda$, the Strehl loss is 44.1 percent (i.e., intensity is reduced to 44.1 percent of the diffraction limited value). To compensate for 15 times worse surface error, the aperture area must scale as $1/0.441 = 2.27 \approx (15/10)^2$. A more meaningful relationship between blur circle diameter and telescope quality, based on point spread function, is summarized in Part II.

It has previously been determined that an array of "small" telescopes of diameter d, each with its own focal plane detector system, is a viable alternative to a large, single aperture (Ref. 1). Life cycle cost analysis of both approaches has apparently not been performed. In 2001, Jet Propulsion Laboratory (JPL) began an investigation to examine the use of a small-telescope array as a replacement for a single large telescope. The conclusions of that study are unknown.

If each telescope has an independent focal plane detector, and that detector is cooled with a closed cycled helium refrigerator, the cost model reflected in Equation (1) requires modification. Single stage Pulse Tube coolers can achieve 35 K, and Stirling cycle coolers can achieve at least 50 K for small lift applications. Gifford-McMahon refrigerators can work under a variety of conditions. For example, the same refrigerator can produce 0.5, 2 and 60 W of cooling lift at 4.2, 10 and 80 K, respectively. Reliability data on mechanical refrigerators is sparse. Some closed cycle coolers have been reported to operate for as long as 6 years (Ref. 3). The cost of a custom 3.3 K refrigerator with 1.5 W of lift is about \$100K. A recent estimate for a turnkey superconducting nano-wire based single photon detector system, operating around ≈1 K, is \$800K (Ref. 16). Commercial systems are appearing on the market with associated cost around \$100K for single channel detectors.

The cost per unit of many types of equipment, such as electric motors, centrifugal pumps, gasoline engines, etc. decreases as production quantity increases. The economy of scale of two-stage (≈1 K class) refrigerators is unknown, but some data exists on single stage coolers as shown in Figure 1 (Ref. 3).

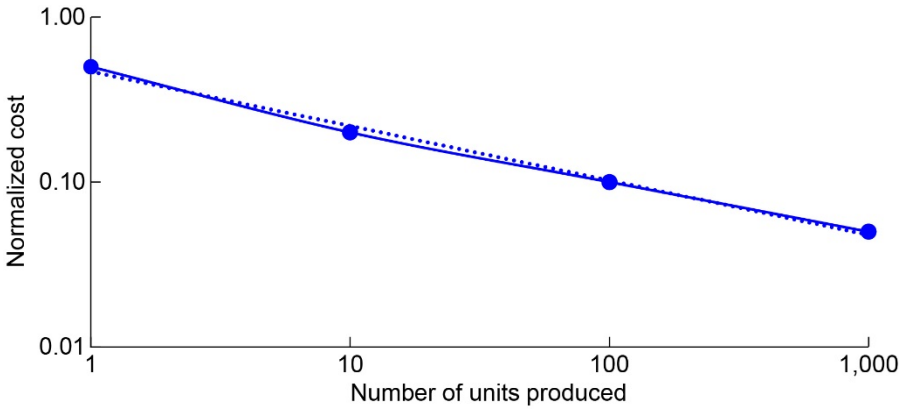

Figure 1.—Estimated cost of single-stage (60 to 80 K) cryocoolers versus quantity derived from (Ref. (3), Figures 8.27).

Estimating the economy of scale from Figure 1 and conservatively taking the cost of a single turnkey superconducting detector refrigeration system as ≈$500K, the cost as a function of quantity (q) is given by:

$$C_R = 0.47q^{-0.33} \tag{2}$$

where C_R is the cost in millions of dollars. Obviously Equation (2) has to be asymptotic to some value but it is assumed to be relevant for the quantities considered herein. It has been estimated that the cost of state of the art space mirrors is $6.4M/m^2. The estimated cost of the 12 m ground telescope to support the Deep-Space Optical Communications system is projected to be around $120M. That includes the telescope and detector system, etc. This estimate is consistent with the cost model presented here as will be shown below. While the cost of a single refrigeration unit is negligible compared to the cost of 12 m optics, in a large array (of relatively small) telescopes, the cumulative cost is not.

A further assumption of the model is that turbulence parameters are constant over the area occupied by the telescope array. According to Reference 2, the performance of an array of small telescopes numbering q is equivalent to that of a monolithic aperture with the same collecting area with diameter D if:

$$q \le \left(D/\mathrm{r_o}\right)^2 \tag{3}$$

where $\mathrm{r_o}$ is the atmospheric coherence length or Fried parameter. The Fried parameter is the area over which the rms wave-front aberration is less than one radian. A typical value (at a preferred observatory site) is ≤15 cm at a wavelength (λ) of 1 μm but there are diurnal and seasonal changes (Ref. 4). (The value of $\mathrm{r_o}$ scales as $\lambda^{1.2}$). Angular resolution is limited by the Fried parameter to $\lambda/\mathrm{r_o}$. The telescope diffraction limit is $\approx\lambda/D$. Since $D >> \mathrm{r_o}$, this explains why adaptive optics are required for imaging ground telescopes. For practical deep-space communications ground stations, $(D/\mathrm{r_o})^2 >> 100$.

Since the effective collecting area of the array must equal the area of the monolithic telescope, $D = \sqrt{q}\,d$. We combine Equations (1) and (2), subject to the constraint Equation (3), to estimate total cost of a telescope array:

$$C = q\left(\alpha\left(D/\sqrt{q}\right)^x + 0.47q^{-0.33}\right) \tag{4}$$

The exponent "x" is taken as the 2.6 per the reasoning in Reference 1, but this may be conservative. It was pointed out in Reference 5 that the exponent has decreased to ≈2.5 for post-1980 manufactured telescopes. Equation (4) does not account for an economy of scale that might naturally occur for

"mass produced" optics and articulation systems. If the mirrors have to be ground and polished to perfection, there may be little reduction in cost per unit. If the mirrors can be cast with minimal post polishing or replicated, there will certainly be value added. For now, it is assumed that this supposed economy of scale is negligible for the quantities under practical consideration here. Figure 2 contains plots of Equation (4) corresponding to three different monolithic telescope sizes, and Figure 3 defines the associated number of telescopes in the array.

The present purpose is to investigate replacing the nominal 12 m telescope proposed to support the Deep Space Optical Communications (DSOC) program. From Figure 2, the minimum cost of $41.9M occurs for a telescope quantity of 141. From Figure 3, the required telescope diameter is 1.01 m.

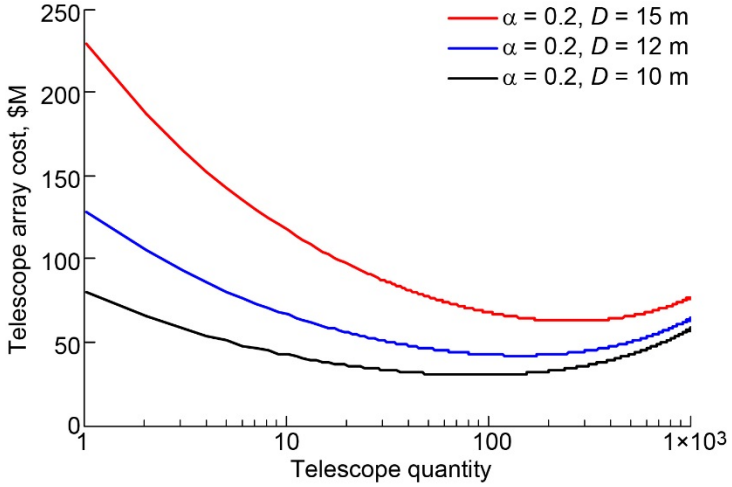

Figure 2.—Estimated telescope array cost as a function of the number of telescopes to emulate a single monolithic 15 m (red), 12 m (blue) and 10 m (black) monolithic telescope. In all cases an $\alpha = 0.2$ is assumed. This corresponds to a 0.5 arcsecond spot size. ($\alpha \approx 0.2$ corresponds to the estimated DSOC 12 m cost).

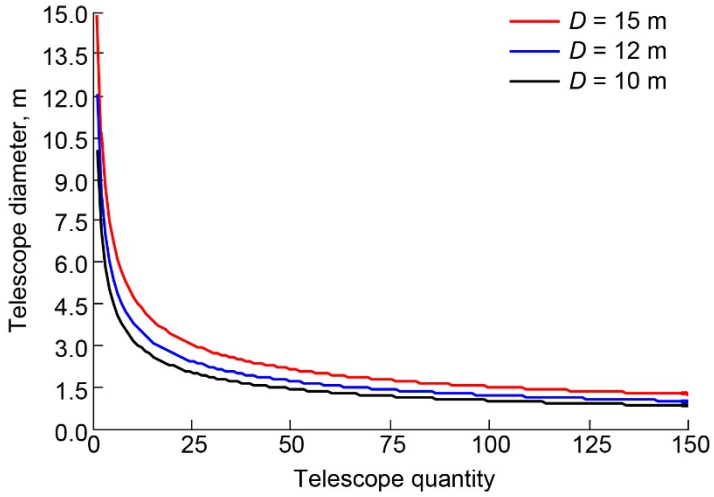

Figure 3.—Corresponding array telescope diameter (m) as a function of telescope quantity for the three different monolithic telescope cases.

An element of cost that has been avoided to this point is the telescope dome, or some protective environmental housing. It has been suggested that for very large telescopes, as the aperture grows, the dome grows as roughly (f# D)^3 (Ref. 5). It turns out that high quality domes are commercially available for ≈2 m class telescopes because of the growing institutional demand for observatories. These come equipped with an electric shutter and motorized dome rotation system (Ref. 6). The standard shutter opening is ≈1.3 m. Weather control is provided by overlapping flanges and temperature regulation is facilitated by the gel coat white exterior. The cost per unit is ≈\$19K. For want of a better model, the dome cost, C_{dome}, is derived from curve fitting data available from Reference 6, as shown in Figure 4. In practice, a high-precision window (e.g., CaF) and a temperature controlled dome would probably be necessary.

As a minimum, the dome diameter must be at least equal to the telescope focal length, assuming the telescope is centered on the pedestal or yoke. Based on the example dome described above, it is assumed that for fast, relatively small telescopes (≤ 2 m) the required dome diameter is $4.6D/\sqrt{q}$. Now including telescope housing cost, Equation (4) becomes:

$$\mathrm{C} \approx q\left(\alpha\left(D/\sqrt{q}\right)^{x} + 0.47q^{-0.33} + D/\left(\sqrt{q}\right)\left(34.6D/\sqrt{q} - 0.026\right) + 0.012\right) \tag{5}$$

A rough estimate of life cycle costs addressing only refrigerator replacement can be approached by assuming half the coolers need to be completely replaced every 5 years. The cost of field maintenance is not included. Using the 12 m aperture requirement, every 5 years 70.5 refrigerators have to be replaced at a cost of \$92K each (from Equation (2) assuming no economy of scale benefit from the prior production run). The results is shown in Figure 5. Once again, the array wins out even for a very long economic life.

The life cycle cost may actually be somewhat greater or less, depending on actual refrigerator reliability, and there may be other maintenance and operating costs not addressed here.

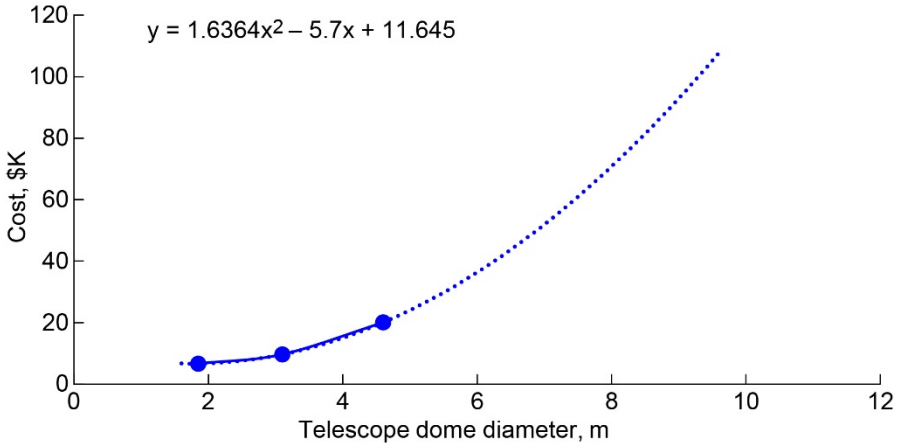

Figure 4.—Estimated cost of telescope enclosure based on commercial grade domes $\left(D/\sqrt{q} > 1\right)$.

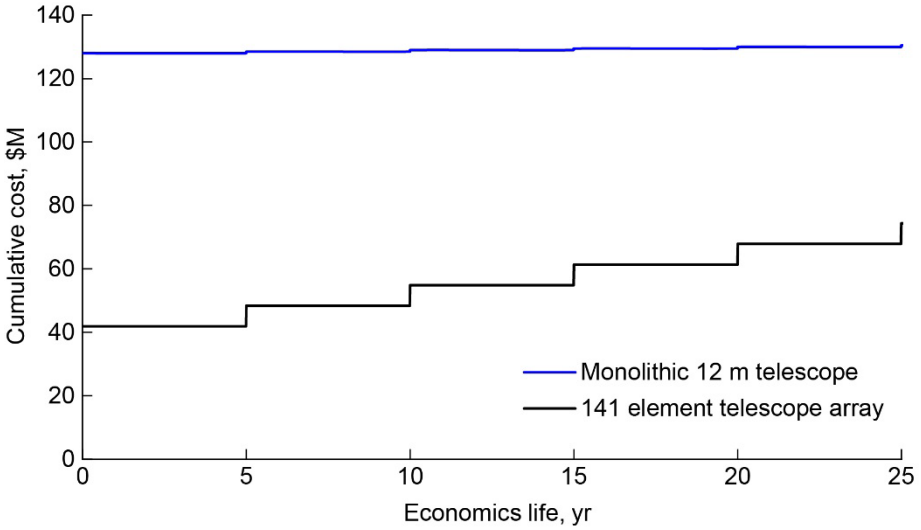

Figure 5.—Estimated life-cycle cost, in today's dollars, of a monolithic 12 m aperture telescope and a 141 element array of 1.01 m telescopes.

Part II. Noise, Turbulence and Imperfect Aperture Considerations

In the case of a microwave receiver, noise coupled in through the antenna is independent of the field-of-view if the observed background has uniform brightness. In general, antenna noise temperature (T_A) is determined by weighting the spatial distribution of background noise temperature with the antenna pattern.

$$T_A = \frac{\int_0^{2\pi}\int_0^{\pi} T_B(\theta,\phi)\sin\theta\, d\theta\, d\phi}{\int_0^{2\pi}\int_0^{\pi} D(\theta,\phi)\sin\theta\, d\theta\, d\phi} \tag{6}$$

where $T_B(\theta,\varphi)$ is sky brightness temperature distribution and $D(\theta,\varphi)$ is the antenna directivity pattern. At radio frequencies, brightness temperature is expressed in terms of background spectral energy density ($B_\nu(T)$) as $T_B = \lambda^2 B_\nu(T)/(2k)$ where k is Boltzmann's constant. $B_\nu(T)$ is measured in units of W m^{-2} Hz^{-1} $Steradian^{-1}$. If the sun is in view, for example, T_A can be affected dramatically - depending on antenna beamwidth. Similarly, if a significant side-lobe observes a hot object (e.g., a building) T_A can increase over the main beam contribution to noise. The noise temperature is referred to the antenna terminals and must also include antenna ohmic loss. Actual noise power is proportional to receiver filter bandwidth (B). Index of refraction changes due to atmospheric turbulence have little effect on detected amplitude at microwave frequencies. The main difference between an optical receiver and a microwave receiver is that in a photon starved link, performance is determined by Poisson statistics. But operation of an optical receiver is essentially similar - background noise collected by a diffraction limited telescope (i.e., no atmospheric turbulence) is independent of aperture size. That is, the noise power is equal to the product of background spectral radiance, filter bandwidth, telescope aperture, and the solid angle (Ω_T) subtended by the telescope field-of-view (FoV). Since Ω_T is inversely proportional to aperture size, noise power is independent of aperture size. This approximation is invalid in the presence of atmospheric turbulence. The magnitude of the turbulence is determined by the atmospheric coherence length, or Fried parameter, r_o. The Fried parameter represents the spatial extent over which the phase of a propagating optical beam is essentially preserved.

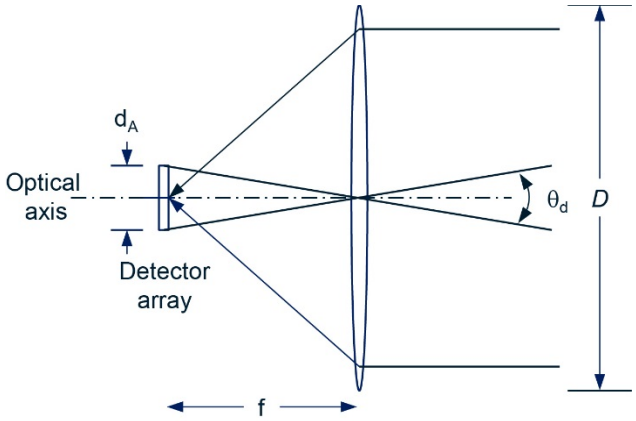

Figure 6.—Geometry of basic telescope system. Note the relationship among beam divergence angle θ_d, detector size d_A, and telescope focal length f.

For a pulse-position modulation scheme using direct detection of single photons at the receiver, field-of-view depends on the focal plane detector size. The field-of-view can be calculated as:

$$\mathrm{FoV}=\left(\text{number of pixels}\right)\times\left(\text{pixel size}/\text{focal length}\right) \tag{7}$$

Referring to Figure 6, the FoV can be increased by using a larger detector chip. In the case of a diffraction limited telescope, the detector element (pixel) size corresponds to the minimum spot size and is generally set to the extent of the Airy disk.

Angular resolution of a diffraction limited circular aperture is:

$$\theta_d = 1.22\lambda/D \tag{8}$$

where the factor 1.22 is derived from the location of the first dark ring of the Airy disk. (1.22 is the first zero of the Bessel function of the first kind, of order one, divided by π.) It is straightforward to convert angular resolution to spatial resolution. From the diagram,

$$\tan\left(\theta_d/2\right)=\left(d_A/2\right)/f \tag{9}$$

or combining Equations (8) and (9)

$$d_A \approx 1.22\lambda f/D = 1.22\lambda f\# \tag{10}$$

An estimate of resolution is generally taken as 2.44 λ f# (the Airy disk is the central bright spot of the Airy pattern and contains 84 percent of the energy and will be discussed more in the subsequent section). From the diagram, an optical system with a small f# (i.e., f/*D*) produces a lower beam intensity (W/steradian) than a system with a larger f# (i.e., suggesting advantages to a long focal length). This is because the beam divergence increases faster than the beam flux (W) as focal length is reduced. Note that "image" brightness scales as D^2 and while a 1 m f/4 telescope has the same focal length as a 2 m f/2 telescope, the latter is four times "faster." Long focal lengths may present primary and subreflector lateral alignment challenges because of mechanical vibrations and thermal distortion.

Atmospheric turbulence can cause the actual FoV (i.e., telescope beam solid angle) to be many times the theoretical diffraction limit – essentially increasing background stray light (e.g., scattered sunlight). The actual spot size or blur circle diameter is greater than the diffraction limited focus because the turbulence induces angle-of-arrival fluctuations causing spot displacement. The turbulence is really random inhomogeneities in the atmosphere's refractive index. It induces an angular beam spread with a radius of approximately λ/r_o (Figure 7).

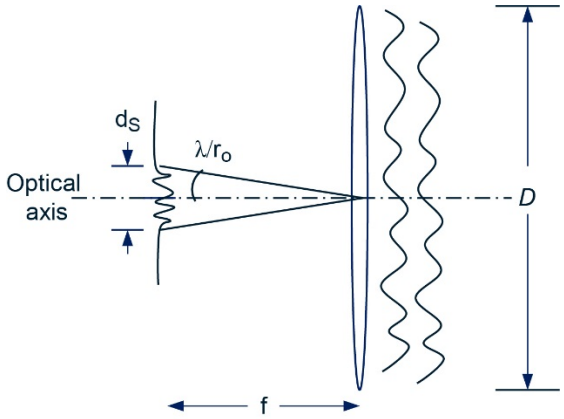

Figure 7.—Geometry of basic telescope system illustrating effect of turbulence on point spread function. Turbulence is regarded as distributing the signal into $(D/r_o)^2$ random spatial modes at the detector plane (Ref. 7).

The focused spot size becomes $d_S \approx 2\, f\, \lambda/r_o$. A larger detector is necessary to encircle the signal energy, which increases the FoV. Since d_S must be smaller than the detector diameter d_A, this implies

$$f \le d_A\, r_o / 2\lambda \tag{11}$$

From a manufacturing point of view, the f# needs to be greater than about 1. (Low f# implies a highly curved parabolic surface which is difficult to manufacture.) This leads to the conclusion:

$$D \le f \le d_A\, r_o / (2\lambda) \tag{12}$$

which can also be expressed as

$$d_A / f \ge 2\lambda / r_o \tag{13}$$

This is near the cusp for a ≈1 m telescope for a 20 cm r_o. That's an important conclusion that may drive the f# slightly below 1. Note that larger detector size will also eventually be an issue due to capacitance.

Equivalent Aperture Sizing

This section analyzes the relationship between aperture size, aperture surface quality and photon collection efficiency. It is based on a surface error model and the corresponding optical point spread function which determines the fraction of signal energy captured by the detector FoV. The model is based on the analysis of Ruze as applied to microwave parabolic reflector antennas, and the work of Sandusky et al. (Refs. 8 and 9). As a practical example, silicon carbide mirrors can be manufactured up to at least 1.5 m in diameters with λ/10 peak-to-valley figure accuracy and 10 Å rms surface roughness using post polishing techniques. But finishing processes (lapping, polishing) for SiC "blanks" are labor intensive, require highly skilled optical technicians, and highly specialized machinery because of the extreme hardness of SiC. Trading surface quality (polishing cost) and aperture size is an important consideration of this study.

The point spread function for a "perfect" optical system is the famous Airy pattern – which is derived from Fraunhofer diffraction theory. The intensity of the Fraunhofer diffraction pattern, I(θ), is given by the squared modulus of the Fourier transform of the aperture, where θ is the observation angle from the optical axis. For a circular aperture with a central circular blockage:

$$I(\theta) = \frac{\left(2 \cdot \frac{J1(k \cdot a \cdot \sin(\theta))}{k \cdot a \cdot \sin(\theta)} - 2 \cdot \varepsilon \cdot \frac{J1(k \cdot a \cdot \varepsilon \cdot \sin(\theta))}{k \cdot a \cdot \sin(\theta)}\right)^2}{(1-\varepsilon^2)^2} \tag{14}$$

I(0) is the normalized maximum intensity, J1 is the Bessel function of the first kind of order one, k is the wavenumber ($2\pi/\lambda$), the radius of the aperture is a, and ε is the fractional radius of the central obscuration of the primary (e.g., the ratio of the sub-reflector radius to the primary mirror radius). For photometric measurements, the encircled energy is used to represent the integrated flux contained within the detector radius $r_A = d_A/2$. The total power contained in the diffraction pattern is obtained by integrating Equation (14). A "real" optical surface has random surface errors which result in scattering and modification of the point spread function (i.e., some of the light scatters at random angles). The Ruze equation is generally used to quantify reflector gain degradation due to randomly distributed surface imperfections (Ref. 8). The mirror is assumed to contain normally distributed surface errors having zero mean and standard deviation σ (i.e., σ is the RMS roughness in terms of λ). It should be pointed out that the Ruze model does not apply to reflectors with very smooth surfaces (i.e., $\sigma/\lambda << 1$) and large shape errors (e.g., membrane modes involving large spherical aberrations near the vertex and flaring of the parabola near the rim due to boundary loading) (Ref. 10). The signal degradation is proportional to the exponential of the square of the RMS surface errors (i.e., $e^{-(4\pi\sigma)2}$). The scattered field also depends on the surface autocorrelation function and the characteristic correlation length τ – also assumed to be normally distributed. Correlation length is basically the horizontal scale of surface imperfections and is material and process dependent. For a perfectly smooth surface, the correlation length approaches infinity. Short correlation lengths imply more rapid vertical variations as a function of horizontal position. The two waveforms (i.e., generated surface roughness patterns with normal distribution) shown in Figure 8 have the same RMS error. But the bottom pattern seems rougher because of the frequency of vertical variations.

As an example, Figure 9 is a profilometer scan of a prototype composite mirror. The scan length is 30 mm, and the vertical positions of the left and right cursor are –5395 and 897 Å, respectively. Hence the peak-to-valley ratio (P-V) is about 0.6 μm (a little over 1/3 λ at 1550 nm). There is no true relationship between P-V and RMS for random surface errors. Diamond turning, for example, results in high frequency components, and certain fabrication processes may result is drastic differences between P-V and RMS numbers. From the horizontal scale, we can infer a correlation length of about 6 mm. These surface imperfections introduce corresponding phase-front deformations (σ_φ) of approximately $2\beta\sigma$ where $\beta = 2\pi/\lambda$ and the factor of 2 arises because the path length is roughly twice the feature size. Correlation length is normalized to λ/FoV. The fraction of optical energy, P_E, focused onto the detector is determined by integrating the modified point spread function over the detector area (Ref. 9). It is assumed that point spread function is centered on the detector array.

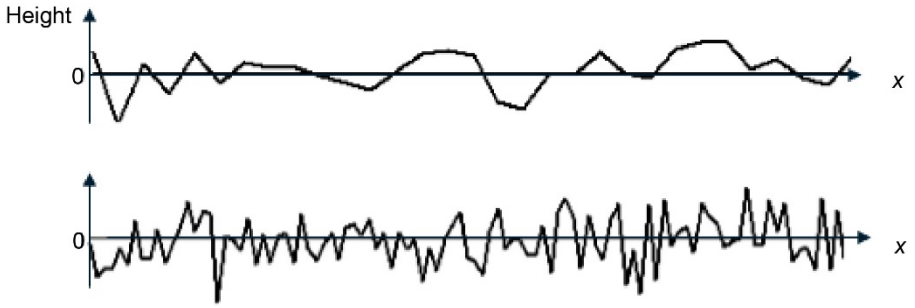

Figure 8.—Two different rough surfaces with zero mean and the same RMS value (σ = 1) but different correlation lengths.

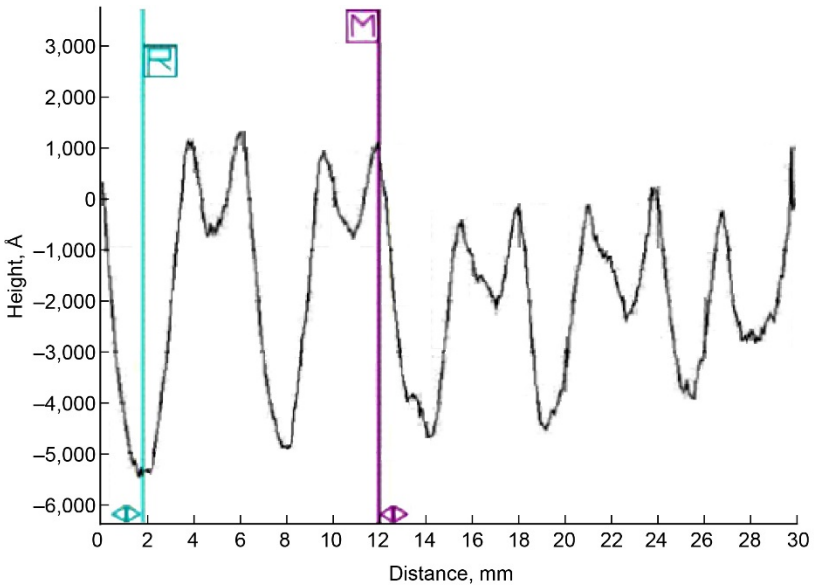

Figure 9.—Profilometer scan of a 7.5 cm composite mirror "coupon". The coupon consists of a 1.8 cm thick aluminum honeycomb core and 0.5 mm thick MJ55 carbon fiber reinforced polymer face-skins. The concave mirror surface (f = 150 cm) has a thin evaporated aluminum coating. The apparent correlation length is about 6 mm (≈300 λ/FoV >> 1 in the example below) (Ref. 11).

For practical purposes, the FoV is large compared to the diffraction limit of the primary aperture as discussed above (i.e., FoV>>λ/*D*). For example, assuming *D* = 1.3 m, λ = 1550 nm, and r_o = 10 cm, d_A = 40 μm. Then, the FoV = 40 μm/1.3 m = 31 μRad. The resolving power of the 1.3 m primary is λ/*D* = 1.2 μRad.

It can be shown that for situations under consideration here (FoV>>λ/*D*)

$$P_E = 1 - e^{-(4\cdot\pi\cdot\sigma)^2} \cdot \sum_{m=1}^{\infty} \frac{(4\cdot\pi\cdot\sigma)^{2\cdot m}}{m!} \cdot e^{-\left(\frac{1}{m}\right)\cdot\left(\pi\cdot\frac{\tau}{2}\right)^2} \tag{15}$$

Now the diameter *D* of a real mirror, required to emulate the performance of a smaller perfect mirror (D_p) in terms of light gathering capacity can be expressed as:

$$D = \frac{D_P}{\sqrt{P_E}} \tag{16}$$

Figure 10 shows tradeoff between scaled primary mirror size and RMS surface roughness with correlation length as a parameter. As an example, consider the composite mirror data provided above. While there is no exact relationship between P-V and RMS for such surfaces, a rule of thumb is that P-V is about four times the RMS error. 1500 Å is actually very close to the average RMS error that was measured for the composite coupons. Using this number and assuming the same FoV (31 μRad) as in the earlier example, the required mirror diameter is essentially equal to that of an ideal mirror. In this case there is no need to compensate for surface aberrations because they have small RMS amplitude (≈λ/10) and the correlation length is >>1. According to the formulation, for long correlation length (τ>1) there is virtually no mirror diameter increase necessary for surfaces with up to a λ/10 RMS error. For relatively smooth surfaces (say σ/λ<0.1), the diameter scaling is essentially independent of correlation length for τ<0.1 λ/FoV. Figure 11 simply expands the region near the knee of the curves.

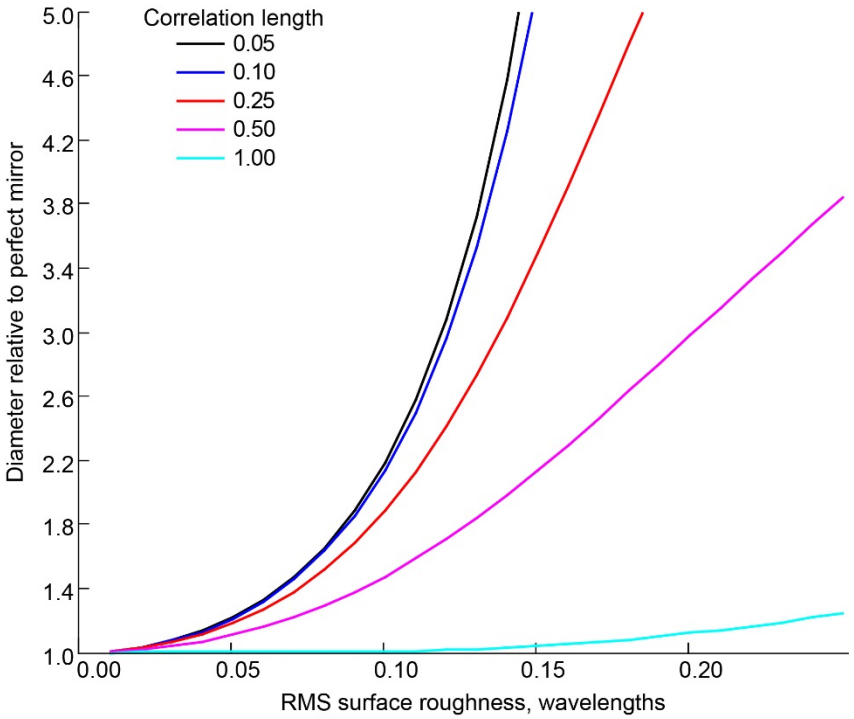

Figure 10.—Manufacturable telescope scale factor relative to a perfect mirror as a function of RMS surface roughness, with correlation length expressed in terms of λ/FoV (i.e., ≈ $\lambda f/d_A$) as a parameter, and RMS surface roughness ranging up to 1/4 λ.

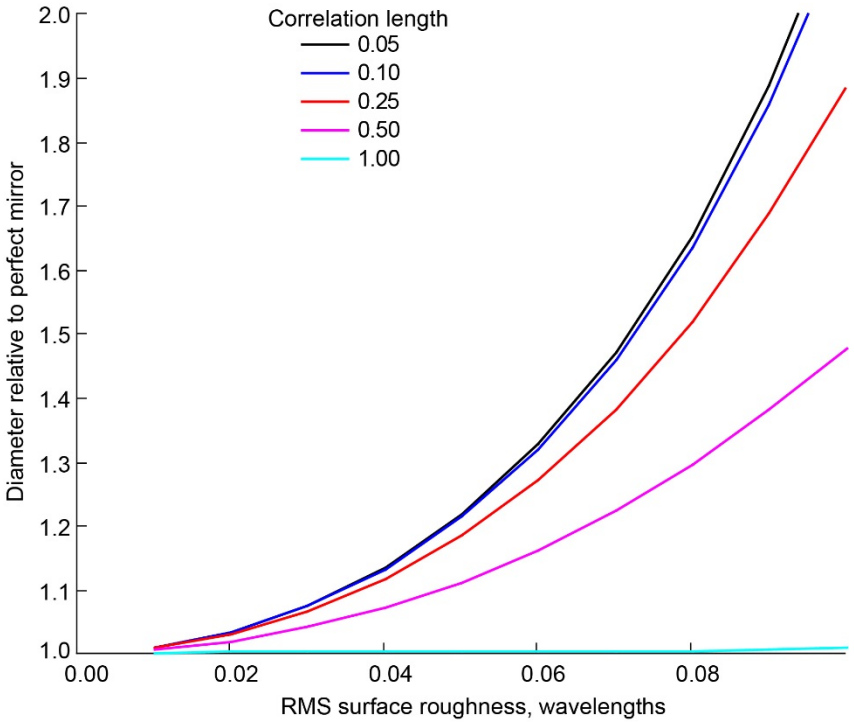

Figure 11.—Manufacturable telescope scale factor relative to a perfect mirror as a function of RMS surface roughness, with correlation length expressed in terms of λ/FoV as a parameter. Expanded view of Figure 10 concentrating on small surface roughness.

Part III. Cost Minimization

Figure 10 and Figure 11 highlight the importance of understanding the spatial frequency content of the imperfect mirror surface. Three distinct regimes exist. Low frequency errors are associated with conventional wavefront aberrations (e.g., spherical aberration). Surface roughness (micro-roughness) introduces wide-angle scattering and reduces signal-to-noise ratio. The so-called "midspatial" irregularities result in small angle scatter and smear the point spread function. Harvey et al. (Ref. 14) describe an effective roughness based on the spatial frequency band limits of the surface. That work also introduces an alternative to a normally distributed surface autocorrelation function. Their conclusions are most applicable to situations involving short correlation lengths ($<\lambda$) and large incidence angles (which would generally not apply to a single photon detecting telescope scenario).

Polishing SiC generally requires a diamond based slurry, and material removal rates are small in comparison to conventional optical materials (Ref. 12). The material removal rate for SiC is less than 5 percent that of conventional materials like fused silica. It can take several months of precision polishing to achieve $\lambda/10$ P-V surface figures and ≈10 Å RMS roughness for even modest size mirrors. Alternatives to direct polishing, such as Xinetics' nanolaminate face-sheet bonding (Ref. 13) or Zygo's magneto-rheological polishing may reduce costs significantly (Ref. 12).

Basis of Cost Estimate

The next step is to relate mirror surface quality to cost, or more precisely to correlate labor and machining intensive post-polishing and cost. Equation (1) was derived from empirical data *representing a broad class of telescope types and sizes*. As a sanity check to estimate relatively small SiC mirror cost versus aperture size and quality, the cost of modest size glass mirrors is used along with the 5 percent scaling factor (i.e., 20X) for SiC. Pricing for high quality glass mirrors is available from R.F. Royce - Precision Optical Components, for example. The raw material of SiC is significantly more expensive than conventional glass blanks (≈35$/kg vs. ≈$1/kg) but this is negligible compared to the fabrication cost. Figure 12 compares Equation (1) with a power law curve fit to small glass mirror cost scaled to reflect SiC post-processing. The small mirror power law curve indicates a roughly 25 percent higher cost in the region of interest. The power law curve is not valid for large mirrors (≈> 3 m).

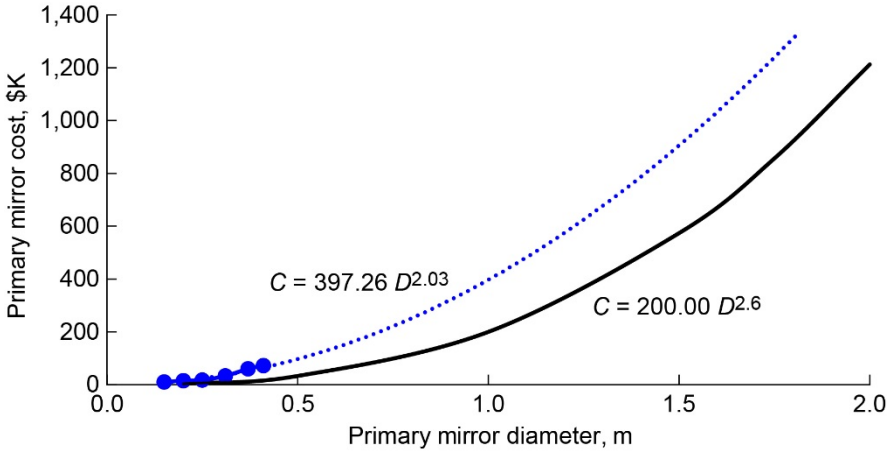

Figure 12.—Mirror cost based on Equation (1) (solid line) compared to data extrapolated from small glass mirrors and scaled to reflect the added complexity of SiC processing (dashed line) in $K. The curves cross at D≈3.3 m.

The following relationship between surface quality and cost is hypothetical. It requires substantiation from mirror manufacturers. Nevertheless the results will be used with the preceding model to generate a final cost estimate. The relationship between surface quality and manufacturing cost can be changed without affecting the approach to the optical array cost minimization problem.

Because of crystal dislocations, porosity, etc. cast (i.e., "off-the-mandrel" so to speak) SiC RMS surface errors can be around 15 μm. Polishing is a process that involves pressure, speed and time. Also, polishing a parabolic surface is much more difficult than polishing a spherical surface. The rate of departure of a parabolic surface from a spherical surface is proportional to D^4/f^3 – suggesting further advantage to smaller mirrors. From the analysis presented in Part II. Noise, Turbulence and Imperfect Aperture Considerations and Figure 10, it can be inferred that a mirror with an RMS error less than λ/100 is essentially indistinguishable from a perfect mirror. This equals 155 Å at a wavelength of 1550 nm. *The cost of the primary mirror is assumed to be inversely proportional to the surface error.* The RMS surface error is assumed to be constrained from 15 μm or about 10λ (unpolished) to 0.0155 μm (extreme polishing).

Based on the initial conclusion that an array of 141, 1.01 m diameter mirrors is *nearly* optimal, the cost of the array should be bounded by:

$$C_H = q \cdot \left[(0.397) \cdot \left(\frac{D}{\sqrt{q}} \right)^{2.03} + 0.47 \cdot q^{-0.33} + \left[\frac{D}{\sqrt{q}} \cdot \left(\frac{D}{\sqrt{q}} \cdot 0.035 - 0.026 \right) + 0.012 \right] \right] \tag{17}$$

on the high side. Using this equation, the projected total array cost is \$73M, with \$57M, \$13M and \$3M attributed to the telescopes, refrigerators and domes, respectively. Equations (15) and (16) or Figure 11 can be used to trade cost of the highly polished SiC mirror with a less perfect but somewhat larger mirror. For example, instead of polishing to a micro-roughness of λ/100, a 1.92 m mirror with a λ/10 micro-roughness could be used (assuming a correlation of 0.25 is feasible), enabling a ≈3X reduction in post-polishing costs. That is, starting with an as-cast 15 μm rms roughness and polishing to 0.15 μm rms roughness instead of 0.015 cuts the time by 1/3 – assuming a linear relationship. This implies an initial investment of about \$55M for the optical ground array, and a 25 year life-cycle cost of about \$85M. If a 2.5 m SiC mirror scaled from a 1.3 m prototype is feasible from a manufacturing perspective and turbulence considerations allow it, the upper cost is slightly lower – about \$51M. In this case, \$38.4M, \$9.2M and \$3.2M are attributed to the telescopes, refrigerators and domes, respectively. And, only 85 telescopes are required. These costs can be further reduced by dedicating one refrigerator to multiple channels (detectors). There is precedent to suggest that at least eight single photon detector channels can be accommodated by a single refrigerator.

The cost curve minima is also very broad – that is over a certain range the cost is largely insensitive to quantity suggesting a further trade between aperture size and quantity.

Other Important Considerations

The correlation between scattered light coupled onto the detector and primary mirror surface roughness also needs to be considered. In particular, the compromise made above may impose restriction on minimum Sun-Earth-Probe angle. Also, since atmosphere turbulence affects even direct detection systems since detector size is affected, cost optimization will be influenced by site location and detector size needs to be chosen based on the specific nominal link condition.

Appendix A.—Manufacturing Technology

Manufacturing alternatives, which will affect the exponent in Equation (1), need to be very carefully considered. Traditional mirror fabrication involves grinding a low CTE glass, the legacy material, or a beryllium blank to spherical shape and coating it with a reflective film. Aerial density ranges from 15 to 25 kg/m^2. The process is limited by the minimum thickness required for grinding. Stiffness is proportional to thickness^2/D. The drive to reduce telescope mirror weight is also directly linked to the fact that the weight of the optics determines the type and weight of the support structure. The focal ratio is also an important economic consideration. Faster mirrors are more expensive to manufacture – longer focal lengths are easier to make because there is less departure from a spherical surface. Traditionally, the ratio of diameter to thickness is about 6:1.

SiC is an excellent candidate material for an array of telescopes: SiC is has 6 to 7 times the stiffness of ULE glass, and also has excellent thermal properties. The process starts with a carbon fiber reinforced plastic blank. The blank is heated (>1000 °C) to create a rigid "green" state. This structure can be relatively easily machined to the required shape – to an accuracy of perhaps 0.1 mm. Once machined, the green structure is heated under vacuum at a temperature allowing silicon to be in a liquid state (T > 1400 °C). The liquid silicon interacts with the carbon to form a Silicon Carbide matrix. SiC attributes include extremely high specific stiffness, high thermal conductivity and superior dimensional stability. The aerial density is 10 to 15 kg/m^2. Because the surface is rough and porous, it is generally re-fired after filing the pores with pure Si. The mirror blank can then be ground (polished) and coated. Modifications to this process include using chemical vapor depositing to coat the surface with SiC to form a very dense encapsulation layer and ion beam polishing to improve the RMS roughness (Ref. 17).

Carbon Fiber Reinforced Polymer (CFRP) composite mirror replication promises aerial density around 2 kg/m^2, and the replication process is inherently intended for mass production. The first step in the optical replication process is to grind and polish a glass mandrel to the inverse of the desired shape (i.e., a convex mandrel is required for a concave mirror). Then, successive plies of graphite-fiber-composite pre-impregnated polymer materials are applied on the mandrel. The resulting laminate is then cured under heat and pressure, released from the mandrel, and vacuum-coated with a reflective coating. Issues with CFRP include shrinkage due to thermal strain and chemical conversion volumetric shrinkage of the adhesives and fiber print-through. NASA GRC is developing a process that eliminates print-through and has demonstrated a surface finish ≈50 Å rms on 7.5 cm composite coupons.

There are also tradeoffs between a monolithic mirror and a segmented mirror. Segmented mirror technology is less expensive, but a monolithic mirror produces a more stable point spread function. Segmented mirrors also have peculiar errors since there will be a correlation length associated with the panel size, as well as local errors on the individual panels. Nevertheless, segmented mirror technology needs to be contrasted with monolithic mirrors.

Appendix B.—Atmospheric Refraction Considerations for Beaconless Pointing

Atmospheric refraction depends on ground station elevation, pointing angle, wavelength, temperature and pressure (and therefor is a function of altitude). The atmospheric model used here (Figure 13) consists of m concentric shells, with shells characterized by a refractive index n_0 to n_m. Here, n_0 corresponds to the index of refraction associated with the ground station (Refs. 18 to 20). The atmosphere (troposphere) is assumed to be 20 km thick (i.e., the index of refraction is unity past 20 km). Index of refraction depends on air density, and air density is a strong function of altitude. So the lengths of the division intervals increase with altitude. Air density is not a strong function of the horizontal direction, so only the vertical structure of the atmosphere is accounted for.

The index of refraction depends on temperature, pressure, and humidity, and the refraction error accuracy depends on the models assumed for those parameters which are a function of altitude. It is generally assumed that the vertical temperature profile rate is –6.5 K/km up to 11 km and constant beyond as shown in Figure 14.

The pressure depends on the assumed temperature lapse rate (from Figure 14). The molar mass of dry air was taken as 0.02896 kg/mol. At very low altitudes the pressure decrease at a rate of about 1.2 kPa per 100 m. The modeled pressure versus altitude shown in Figure 15 ignores this rapid change since the ground terminal is several hundred meters above sea level.

The index of refraction derived from the above models is shown in Figure 16. The absolute accuracy of the models is not the point here. The resulting magnitude of the refractive error is. The numerical procedure for determining the refracted path was implemented in MathCAD.

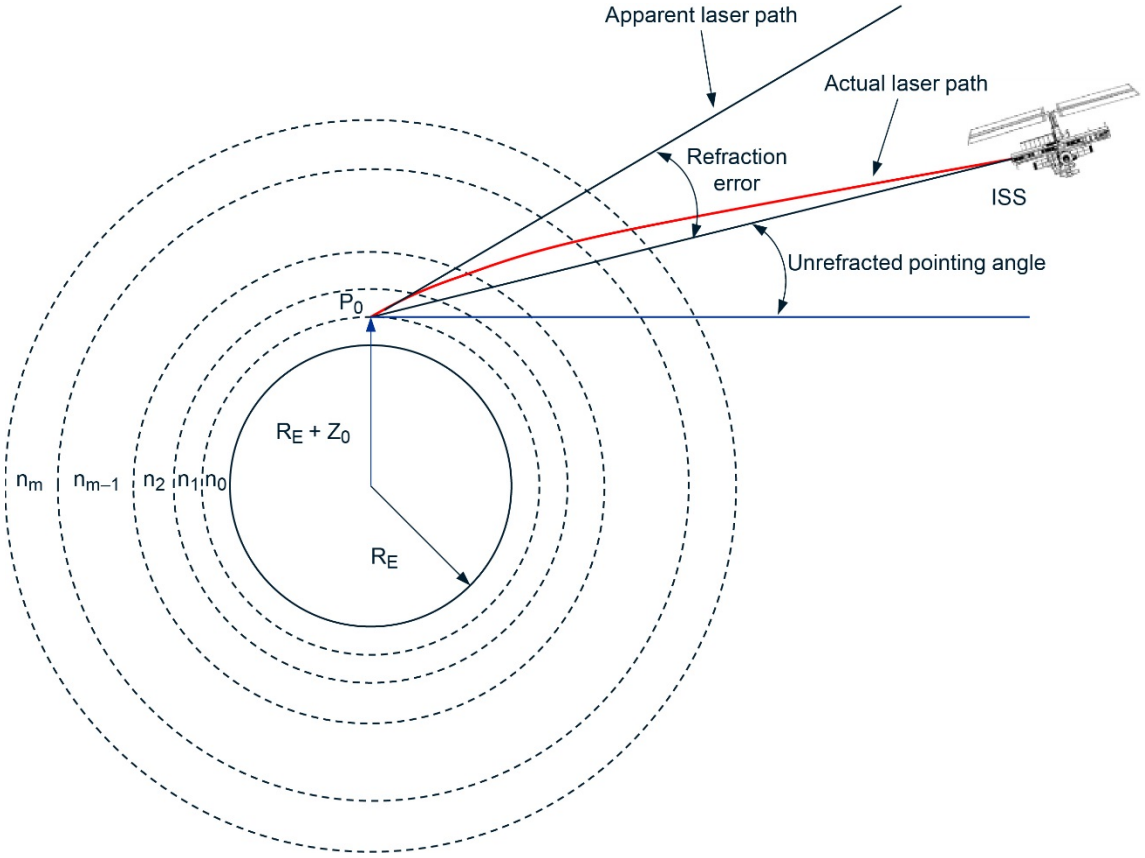

Figure 13.—Atmospheric refraction model. The radius of the Earth is R_E and the elevation of the ground station is Z_0 and $n_0 > n_1 > \ldots n_m$. The apparent laser path is the tangent line to the final actual laser path refraction angle.

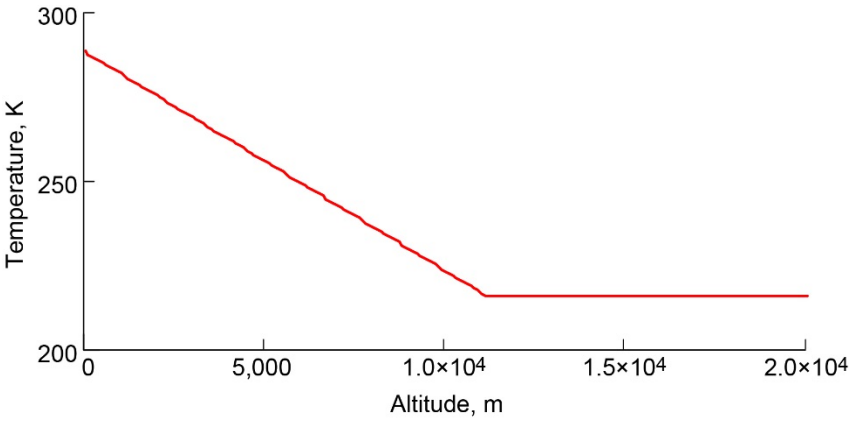

Figure 14.—Modeled vertical temperature profile.

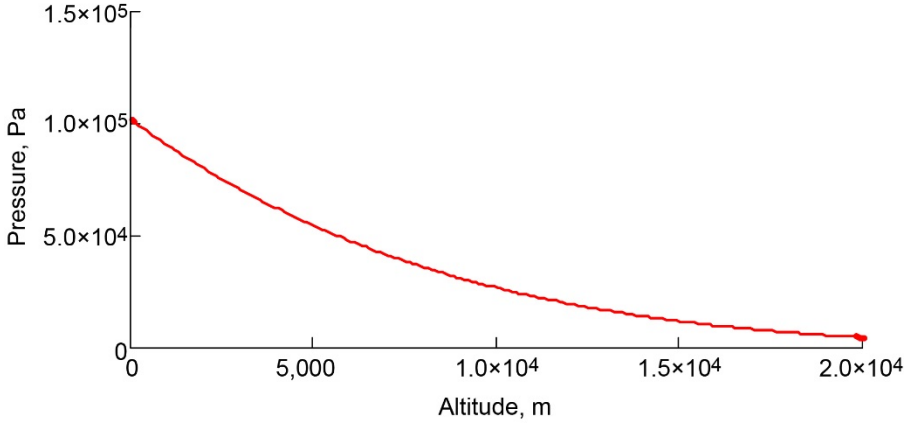

Figure 15.—Modeled pressure profile.

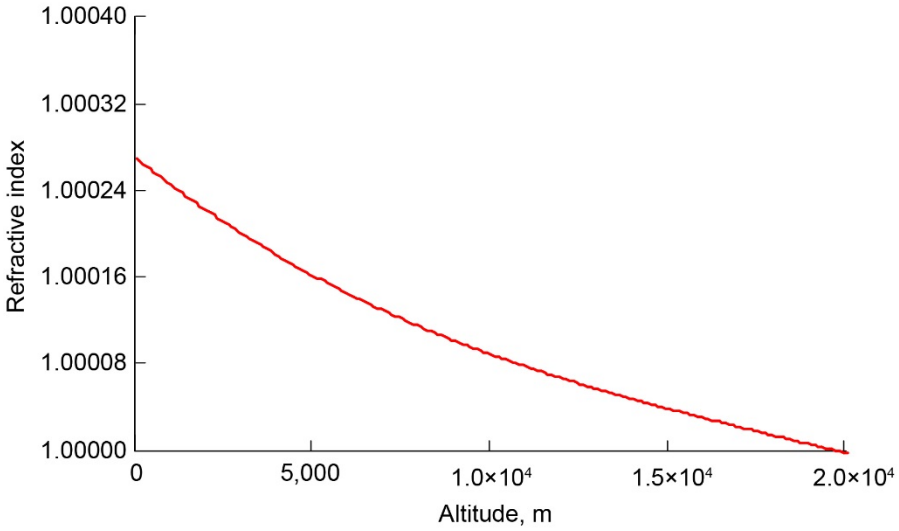

Figure 16.—Calculated index of refraction as a function of altitude. The results correspond to a Cleveland, Ohio observation point (elevation = 241 m), a wavelength of 1550 nm, a humidity of 10 percent up to 2 km and 0 percent humidity beyond.

The final results are shown in Table 1 for two very “extreme” pointing angles: 10° and 80° above the horizon. Two cases were run for each angle: a static case (no atmospheric refractive index fluctuations) and a dynamic case (where the index was allowed to fluctuate by 0.01 percent). The second and third columns should be identical and it is presumed they would be if a sufficient number of runs occurred. The shell slant range (Figure 13) was 100 m.

In principle, this predictable error could be built into a calibration table for pointing. The result would have to be verified via experiment to lend credibility to the table. Then, only the variance would be of concern. The atmospheric refraction error for several ground station locations is shown in Figure 17.

TABLE 1.—REFRACTIVE POINTING ERROR AS A FUNCTION OF POINTING ANGLE

Pointing angle, degrees	Static refractive error, arcseconds	Average dynamic refractive error, arcseconds	Standard deviation, arcseconds
80.0	5.27	5.34	0.13
60.0	16.41	15.79	0.80
30.0	38.54	37.94	1.41
10.0	70.46	68.63	6.87

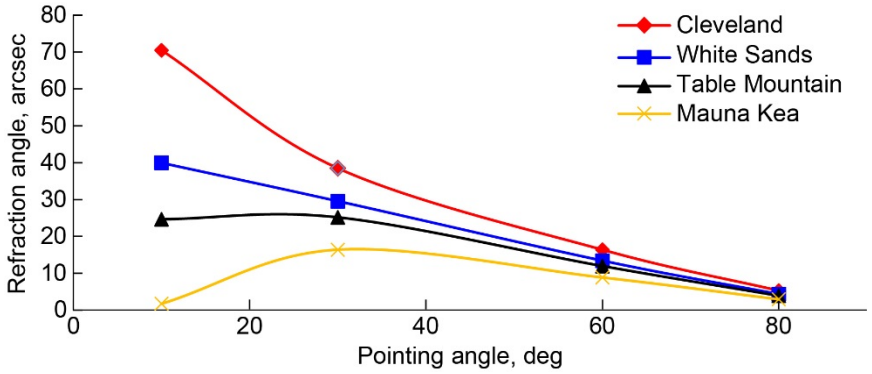

Figure 17.—Atmospheric refraction error for several ground station locations as a function of pointing angle.

References

1. "A Cost-Performance Model for Ground-Based Optical Communications Receiving Telescopes," J.R. Lesh and D.L. Robinson, *The Telecommunications and Data Acquisition Progress Report 42–87, July–September 1986*, Jet Propulsion Laboratory, Pasadena, California, pp. 56–64, November 15, 1986. http://ipnpr.jpl.nasa.gov/progress_report/
2. "Deep Space Optical Communications," Hamid Hemmati, Editor, Jet Propulsion Laboratory California Institute of Technology, Deep Space Communications and Navigation Series October, 2005.
3. "Low Temperature Electronics: Physics, Devices, Circuits and Applications," E. Gutierrez, M. Deen and C. Claeys eds., Academic Press, 2001, pp. 932–933.
4. "Deep Space Optical Communications," Hamid Hemmati, Editor, Jet Propulsion Laboratory California Institute of Technology, Deep Space Communications and Navigation Series October, 2005, pp. 480.
5. "The Scaling Relationship Between Telescope Cost And Aperture Size For Very Large Telescopes," Gerard T. van Belle; Aden B. Meinel and Marjorie P. Meinel, *Proc. SPIE* 5489, Ground-based Telescopes, 563 (September 28, 2004).
6. http://www.optcorp.com/tt-pd15-pro-dome-15-observatory.html
7. Personal Communication, Paul Shubert (Schafer), July 10, 2015.
8. "Antenna Tolerance Theory," J. Ruze, Proc. IEEE, vol. 54, pp. 633–640, April, 1966.
9. "Deep-Space Optical Reception Antenna (DSORA): Aperture Versus Quality," J. Sandusky, D. Hoppe, and M. Britcliffe, TMO Progress Report 42-143, November 15, 2000.
10. "The Effect of Boundary Support and Reflector Dimensions on Inflatable Parabolic Antenna Performance," M. Coleman, F. Baginski and R. Romanofsky, NASA/TM—2011-217110, November, 2011.
11. Data taken by Nick Varaljay on Dektak stylus profilometer, NASA Glenn Research Center, May, 2015.
12. "Rapid Fabrication of Lightweight Silicon Carbide Mirrors," J. Johnson et al., Proceedings of SPIE vol. 4771 (2002), pp. 243–253.
13. US Patent # 7195361 B2, Hybrid Optical Component, M. Ealey, 2007.
14. "Total Integrated Scatter from Surfaces with Arbitrary Roughness, Correlation Widths, and Incident Angles," J. Harvey et al. Optical Engineering, vol. 51, January 2012.
15. "Ground Based Astronomy A Ten Year Program," National Academy of Sciences – National Research Council, Washington, DC, 1964.
16. Personal Communication, Matthew Shaw (JPL), February 26, 2015.
17. "Lightweighted Telescope Mirrors: Outstanding properties of Silicon Carbide," Tutorial Opti521 T. Kashmira, 12/5/2011.
18. "Astronomical Refraction," M. Thomas and R. Joseph, Johns Hopkins APL Technical Digest, vol. 17, Number 3, 1996, pp. 279–284.
19. "A Direct Method for the Calculation of Astronomical Refraction," M. Lipcanu, Proceedings of the Romanian Academy, Series A, Volume 6, Number 2, 2005, pp. 1–7.
20. http://emtoolbox.nist.gov/Wavelength/Edlen.asp